Characterization of Seven Power-Generating Turbine Rotors Using Microscopy-Based Techniques

D.R.G. Mitchell and C.J. Moss

(Submitted 16 March 1998; in revised form 12 May 1998)

Seven turbine generating rotors, either currently in service or recently retired, have been metallurgically examined using nondestructive techniques, including hardness testing and replication for optical and transmission electron microscopy. The aim has been to understand the microstructural changes occurring in a range of rotors due to service exposure. A decrease in hardness of up to 7% was noted, possibly arising from carbide-induced loss of molybdenum from solid solution. Optical microscopy was unable to detect service-induced microstructural changes. However, fine scale secondary precipitation of MC and M_2C were observed using transmission electron microscopy. A range of carbide compositional parameters associated with M_3C were found to vary with service exposure time.

Keywords chromium-molybdenum-vanadium steels, microscopy, power generation, turbine steels

1. Introduction

At the present time, some 70% of power-generating rotors in Australia are over 15 years old, and 50% are over 20 years old (Ref 1). While some of these rotors will be removed from service with the introduction of new plant, many are likely to remain in service for some time to come. Additionally, the recent privatization of sections of the Australian power industry makes extended operation of existing plant seem increasingly likely. Competition is also likely to increase the effective aging rate of plant, owing to more flexible operation.

Turbine rotors, operating at high temperatures and stresses, are critical items of power-generating plant because of large financial losses associated with unscheduled downtime, safety and licensing requirements, high capital costs, and long lead times for replacement manufacture. The cost benefits of avoiding premature retirement can be quite considerable.

Historically, rotors have been made from 1Cr-1Mo-0.25V (1CMV) low-alloy steel, heat treated to produce a fine dispersion of vanadium carbides, and therefore good creep properties (Ref 2). However, owing to compositional and microstructural inhomogeneity in such large forgings, combined with the various temperature and stress regimes found across the rotor, the degradation of the properties due to time in service is complex. Damage mechanisms can involve interactions between creep and fatigue in high temperature regions, while embrittlement, in intermediate temperature regions due to tramp element segregation, can also be a factor. Microstructural modification due to in-service use may involve carbide coarsening, transformation, spheroidization, or secondary precipitation (Ref 3-5), all of which exert an influence on mechanical properties. These microstructural changes are generally too fine to resolve with optical microscopy (Ref 3). Transmission electron microscopy of a rotor steel operated at 288 °C for 23 years showed no modification (Ref 4). In regions of the same rotor that were operated at 500 °C, however, changes in the population of carbides have been found, with secondary precipitation of intragranular M_2C and M_3C, large $M_{23}C_6$ particles forming along prior austenite grain boundaries, and coarsening of MC (Ref 6), where M represents one or more transition series elements.

The presence of four main metallic elements in the alloy (iron, chromium, molybdenum, vanadium) leads to quite complex carbide chemistry, with up to six different carbide types possible, each with a range of solubilities for the main constituent elements (Ref 7). These may include MC (M_4C_3), M_2C, M_3C, M_6C, M_7C_3, and $M_{23}C_6$. The principal carbide in the forging at the start of manufacture is iron-rich M_3C, although with time at temperature, the carbide population shifts toward more thermodynamically favored species, with the stability of carbides formed from the various elements following the sequence V > Mo > Cr > Fe (Ref 8).

While detailed microstructural and microanalytical characterization of laboratory-aged 1CMV steels have been carried out (for example, see Ref 6, 9), few detailed comparative microstructural and microanalytical studies of in-service or ex-service rotors appear in the literature (Ref 3-5). This paper reports some of the microstructural and metallurgical assessments that were carried out on a total of six in-service rotors and one retired rotor, with service exposures of up to 150 kilohours (kh), or over 17 years.

2. Experimental Procedure

A range of 1CMV rotors of various designs, ages, and manufacturers (designated A to G in Table 1) were selected. Access to rotors was achieved during routine turnarounds while other rotor-casing inspection or refurbishment work was being carried out. Excision of even small metal samples from the in-service rotors was not possible. The techniques of examination, therefore, had to be nondestructive. These involved conven-

D.R.G. Mitchell and **C.J. Moss,** Materials Division, Australian Nuclear Science and Technology Organization, PMB 1, Menai, NSW 2234, Australia (C.J. Moss presently at HRL Technology, 677 Springvale Road, Mulgrave, Victoria 3170, Australia). Contact D.R.G. Mitchell at e-mail: drm@ansto.gov.au.

tional nondestructive testing techniques, replication for optical and transmission electron microscopy, and hardness testing.

In general, original test certificate data on rotor composition and properties were not available. In many cases, detailed thermal histories were absent: the number of hours of service exposure being estimated from operational records. This was complicated by rotors having been moved among different units, and by changes in operating conditions. This unavoidable uncertainty in operating data contrasts this work sharply with highly controlled accelerated thermal aging laboratory studies on 1CMV which were often carried out on a single heat (e.g., Ref 6, 9), and is taken into consideration in interpretation of the results.

Regions on the rotors selected for examination were on steam inlet (≈540 °C) and steam outlet (≈350 °C) disks. Throughout this paper, these regions will be referred to as "Hot" and "Cold" sections, respectively. Areas for optical replication were prepared by lightly grinding off the adherent magnetite layer, followed by standard metallographic preparation. Hardness was determined using a portable Equotip (Proceq Zurich, Switzerland) Hardness Tester. Etching was carried out with 5% nital until the surface was mat gray and no longer reflective.

Extraction replicas for transmission electron microscopy were prepared by re-etching the same regions much more deeply to liberate carbides at the surface. Typical etching times were ≈45 s, yielding a very dull mat surface. Replicas were examined using a JEOL (JEOL USA, Inc, Peabody, MA) 2000FXII transmission electron microscope (TEM) operating at 200 keV. Quantitative analysis of carbides was performed using a Tracor Northern EDX system (Noran Instruments, Inc., Middleton, WI), with K factor calibration achieved using appropriate silicide and titanate reference materials.

Table 1 Rotor details

Rotor	Origin	Power, MW	Type	Temp, °C	Hours, kh
A	U.K.	120	HP	540	58.7
B	U.K.	120	HP	540	77
C	Japan	660	IP	522	102
D	Germany	123	HP/IP	538	128
E	U.K.	200	HP	568	136
F	Japan	350	HP/IP	538	149.6
G	U.K.	350	HP	545	150

3. Results

3.1 Hardness and Microstructural Characterization

Hardness data are detailed in Table 2. Typical Cold section hardness values were ≈240 HV. The greatest degree of thermal softening (18 HV) found in the Hot section was for Rotor G. This corresponded to only a ≈7% change in hardness after 150 kh service. The normalized hardness (normalized with respect to the Cold section hardness) as a function of service hours (Fig. 1) showed that softening in the Hot sections with respect to the Cold sections increased with exposure time, albeit with considerable scatter. The corresponding plot of normalized hardness as a function of Larson-Miller parameter, LMP = $T(15 + \log t)$, where T is absolute temperature and t is time (in h), showed no useful trends. The likely reasons for this are discussed in section "4. Discussion."

Table 2 Vickers hardness values of rotor Hot and Cold sections

Section	A	B	C	D(a)	E	F	G
Hot	Not available	241 ± 3	236 ± 3	221 ± 1 (229 ± 2)	219 ± 2	Not available	247 ± 2
Cold	Not available	240 ± 1	236 ± 3	227 ± 1 (232 ± 2)	226 ± 2	Not available	265 ± 3
Hot/Cold	…	1.002 ± 0.016	1.000 ± 0.025	0.974 ± 0.013 (0.987 ± 0.017)	0.969 ± 0.018	… …	0.932 ± 0.019

(a) IP section values are in parentheses

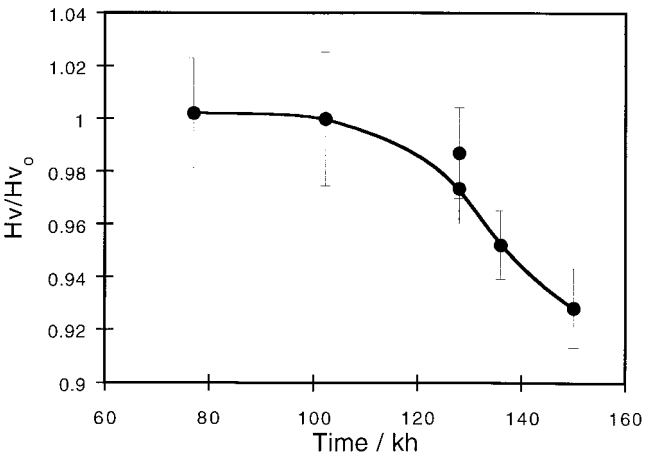

Fig. 1 Normalized change in rotor hardness as a function of service exposure, showing thermal softening

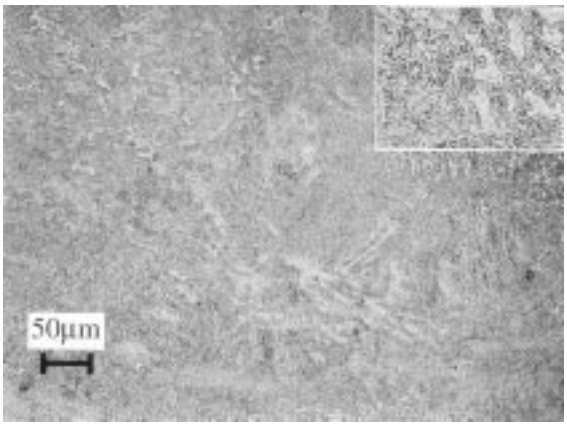

Fig. 2 Optical micrograph of the Hot section of Rotor F (149.6 kh). The microstructure is predominantly upper bainite. Inset is a detail (magnified 4×). Art has been reduced to 34% of its original size for printing.

In all cases, microstructures were found to be predominantly upper bainite. All of the optical microstructures examined were quite similar, with a typical example shown in Fig. 2. Typical prior austenite grain sizes were in the range 10 to 40 μm (ASTM grain size 9 to 10). Examination of individual rotor disks at four circumferential locations 90° apart showed no apparent variation in microstructure. Similarly, examination of different temperature regime locations on individual rotors did not identify any significant microstructural differences. No carbides >5 μm in diameter were seen in any of the rotors studied, nor was there any evidence of creep voids. The typical carbide dimensions were ≈1 μm, being close to the limit of resolution for optical microscopy.

TEM microstructural characterization of all the rotors studied was carried out. This included assessments of homogeneity around individual rotor disks, as well as characterization of Hot and Cold disks along the rotor axis. No significant circumferential segregation effects were observed in any of the rotors. Typical microstructures of Hot and Cold sections from rotors of various vintages are shown in Fig. 3 to 5.

The Cold section of Rotor B, which had undergone only 77 kh of service exposure, exhibited an upper bainitic microstructure, with the majority of carbides being iron-rich M_3C, ≈2 μm in dimensions (Fig. 3a). Prior austenite grain boundaries were difficult to discern, although they tended to be delineated by holes, where slightly larger carbides failed to extract from the matrix during replication. In the corresponding Hot section of the same rotor, the general microstructure was quite similar (Fig. 3b), except for a background of very fine carbides. Energy dispersive x-ray (EDX) analysis showed these to be predominantly MC carbides. These were typically small square platelets being <50 nm in dimension (Fig. 3c). The fine-scale carbide nucleated and grew both within clusters of larger M_3C laths and in the regions between such clusters. The relatively inhomogeneous particle distribution precluded quantitative measurement of particle densities. Two other important carbides were present. Intermingled with the fine-scale MC platelets were short (≈30 nm) rod-like carbides (arrowed), which were found to be rich in molybdenum and were probably early stage precipitates of M_2C. Also present was the composite H-type carbide. Detailed quantitative studies on these particles were undertaken and are described later. The fine-scale MC and M_2C were generally absent or present in very low numbers in the Cold section of this rotor, and it is concluded that these particles are secondary precipitates formed as a consequence of service exposure.

The microstructure of Rotor E (130 kh) showed the Cold section to comprise upper bainite consisting of short (≈2 μm) laths of M_3C (Fig. 4a). Prior austenite grain boundaries were delineated by a few slightly larger holes formed by failed extraction of boundary carbides. There was little to distinguish this microstructure from the Cold sections of the other rotors examined (e.g., Fig. 3a). Fine-scale precipitation was not present in significant amounts. The Hot section of this rotor (Fig. 4b) showed the usual bainitic M_3C laths, and, once again, a high density of fine-scale precipitates similar in composition and morphology to those seen in the Hot section of Rotor B (Fig. 3c).

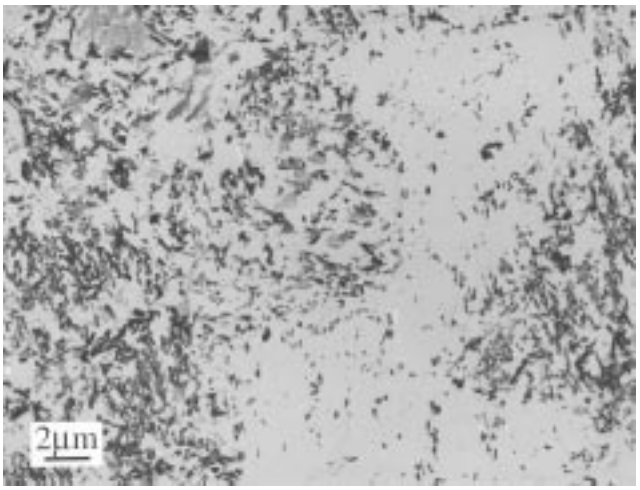

(a)

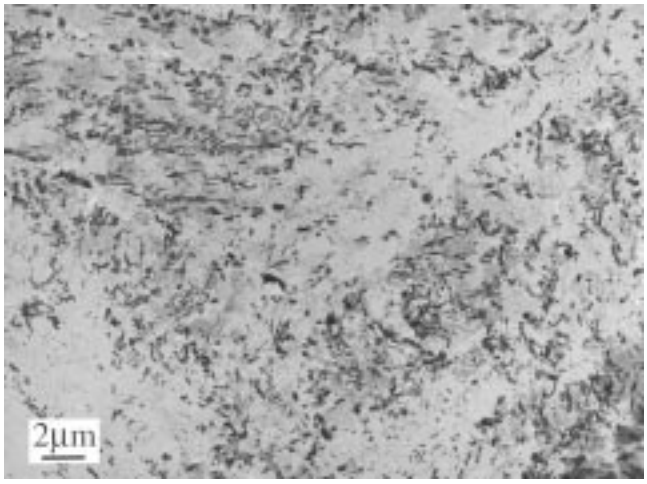

(b)

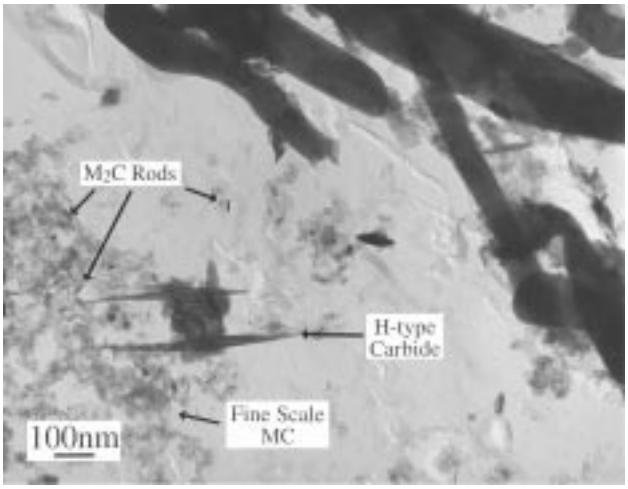

Fig. 3 (a) TEM micrograph from Rotor B (77 kh) Cold section exhibiting an upper bainitic microstructure comprised mainly of M_3C carbides. (b) TEM micrograph from Rotor B (77 kh) Hot section showing a microstructure similar to Fig. 3(a) but with a background of very fine MC/M_2C carbides also present. (c) Detail of Fig. 3(b) showing the fine-scale M_2C (rods) and MC (square platelets) precipitation among clusters of large M_3C laths. An H-type carbide is also present.

In one of the longest exposure rotors studied (Rotor F, 149.6 kh), a similar picture emerged, with bainitic M_3C present in the Cold section of the rotor (Fig. 5). Some fine-scale carbide precipitate was present, being mainly nucleated on the larger M_3C particles. This rotor showed a much lower level of fine-scale carbide precipitation in the Hot section (not shown).

To understand the carbide changes occurring in these rotors due to exposure at service temperature, a wide range of carbide parameters was studied. Fine-scale carbide density measurements were impractical, owing to the different etching responses of the rotors during replication, and due to the difficulties of accurate control during on-site replication. One set of carbide parameters which proved relatively easy to measure were the dimensions of H-type carbides (e.g., Fig. 3c), which were easily recognized due to their distinctive morphology. The parameters measured included: density of H-types relative to M_3C (based on random line intercepts); average M_2C "wing" length; average core dimensions; and various ratios of such parameters for Rotor B. When confidence limits were taken into account, none of the parameters measured showed statistically significant differences between the Hot and Cold sections. A major problem with measurements of this type is the high degree of scatter, often with error limits approaching 50% of the parameter value.

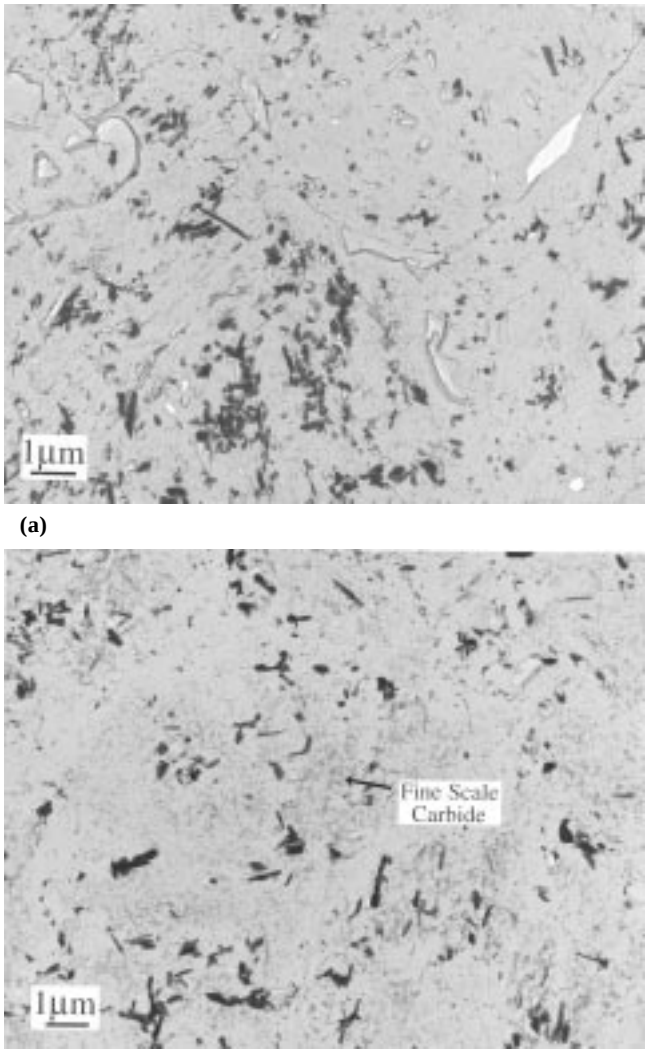

Fig. 4 (a) Cold section of Rotor E (136 kh) showing upper bainitic microstructure of M_3C, with little fine-scale precipitation apparent. (b) Hot section of Rotor E (136 kh), showing a high density of fine-scale precipitation between the M_3C laths

3.2 EDX Analysis

An initial sorting exercise was carried out to identify any carbides persisting in the rotors that were compositionally sensitive to service exposure time. Carbides were identified using chemical compositions derived from EDX measurements, identification based on electron diffraction being too time-consuming to analyze a reasonable number of particles. The use of EDX to identify carbides has been demonstrated by comparative studies with electron diffraction (Ref 13). The following compositional criteria were developed in the present study to identify and sort carbides:

- MC—distinctive morphology, either as ≈25 nm square platelets, or as more massive 100 to 200 nm rectangular cores of H-type carbide; >63 wt% V, molybdenum as other major element.
- M_2C—distinctive morphology, either as short (10 to 50 nm) rods, or as "wings" on the sides of H-type carbides; >75 wt% Mo, vanadium as other major element.
- M_3C—short 1 to 2 μm laths or as rounded globular particles (≈1 μm); non-unique morphology, containing 61 to 73 wt% Fe and 18 to 23 wt% Cr.
- $M_{23}C_6$—small (≈1 μm) particles with a nondistinctive morphology; few particles located, and only in the Hot sections of the rotors; Fe≈Cr = 35 to 42 wt%.
- M_7C_3—none detected here. The literature (Ref 7) suggests a high chromium content (≈50 wt%) for this carbide, although it is likely to be a minority phase, if present at all (Ref 4, 7).
- M_6C—none detected here. The literature (Ref 7) suggests a high molybdenum content (>50 wt%) for this carbide, although it is likely to be a minority phase, if present at all (Ref 4, 7).

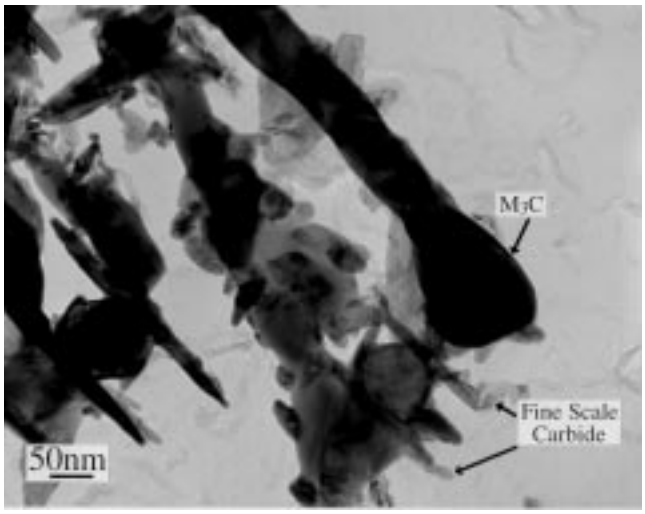

Fig. 5 Cold section of Rotor F (149.6 kh) showing upper bainitic M_3C, with very limited fine-scale precipitation being nucleated on the larger M_3C particles

Studies on both short-term and long-term exposure rotors (Rotors B and G) showed that the composition of M_2C and MC carbides measured in the Cold sections were identical (within error limits) to the respective phase in the corresponding Hot sections. Consequently, these carbides were omitted from further study. Although several carbide types can be found in 1CMV (Ref 7), many of these, such as M_6C, tend to occur only after very extensive tempering, or, like M_7C_3, are rarely if ever found (Ref 4, 7). Therefore, their composition cannot be monitored through the bulk of the service life. However, their presence or absence may be a useful end-of-life indicator. Studies on Rotor G (150 kh) showed that while chromium-rich $M_{23}C_6$ was detected in very limited numbers in the Hot section, none was present in the Cold section, and so once again measuring changes in this carbide's composition between the Hot and Cold sections was not feasible.

The principal carbide in the rotors was the iron-rich M_3C. During analysis, particles were selected at random, ensuring that they were neither too thick for quantitative microanalysis, nor oriented close to a strong Bragg diffraction condition. Any particles which were clearly not M_3C were ignored. Typically 20 to 30 analyses per replica were carried out. The count rate chosen was such that the detector dead time did not exceed 25%, with a counting time sufficient to produce an iron $K\alpha$ peak integral of 20,000 counts.

3.3 M_3C Compositional Parameters

The compositional parameters associated with M_3C were studied extensively. Preliminary studies here and elsewhere (Ref 4, 17) indicate that carbide types found in 1CMV (other than M_3C) are compositionally stable. The majority of the M_3C carbides studied were of fairly similar shape and size, being rounded or lath-like and in the size range of 0.5 to 2 μm. Modeling and experimental studies by Bhadeshia et al. (Ref 10, 11, 15) have indicated that there is a compositional dependence on size, and that this must be taken into account when measuring carbide composition. However, the correlation between size and composition appears to be subject to very considerable scatter (Ref 10, 15). To understand whether carbide size was a factor in the present study, it was measured using the projected area of the particles from Rotor B. The trends for iron, chromium, and manganese as a function of particle area for the Hot and Cold sections are shown in Fig. 6(a) and (b).

In the Cold section (Fig. 6a), the compositional correlation with size was very weak, with some scatter. The best fit index obtained from linear regression of the data was $R = 0.26$ for the chromium data, which showed an increasing amount of the element in the larger M_3C carbides. In the Hot section carbides, there was less chromium and manganese in the larger particles (Fig. 6b), which were correspondingly richer in iron. However, the trends were still weak with considerable scatter. The best fit index obtained from linear regression of this data was for manganese, with $R = 0.37$. In view of the scatter measured in this data, the weakness of the size effect on composition and the time-consuming nature of particle size measurement, all subsequent measurements were made without consideration to particle size, although exceptionally small (<0.2 μm) or large (>2 μm) particles were omitted from the study.

3.4 General Compositional Changes

Plots of the iron, chromium, and manganese content of M_3C carbides as a function of service exposure in both the Cold and Hot sections of the rotors are shown in Fig. 7. It was apparent that compositional change was occurring in the Cold sections, with chromium and manganese enriching at the expense of iron. Because all the rotor Cold sections operate at ≈350 °C, this temperature was clearly sufficient to permit compositional modification, albeit at a slower rate than was observed in the Hot section carbides. It might be assumed that the Cold sections of the rotor represent a snapshot of the likely starting condition of the rotor. Based on the present evidence, however, such an assumption is clearly not valid.

The compositional change as a function of service exposure was greater in the Hot section carbides, with chromium and manganese enriching in M_3C at the expense of iron. The princi-

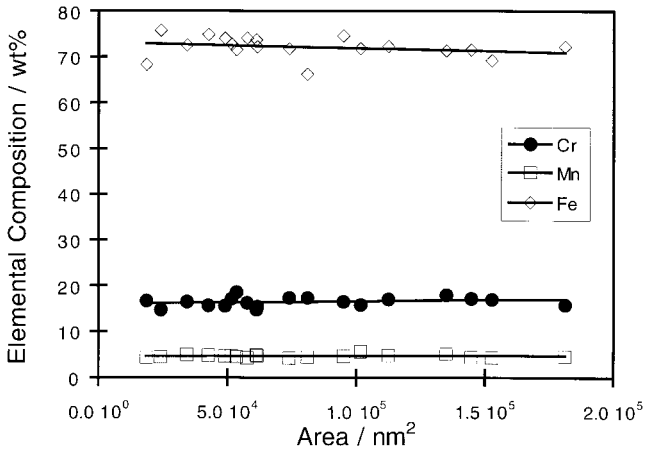

(a)

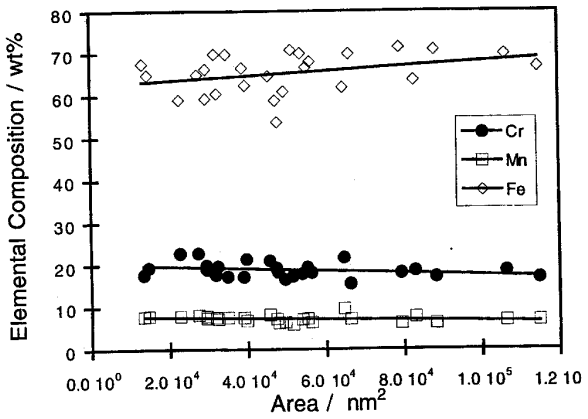

(b)

Fig. 6 (a) Fe, Cr, and Mn content of M_3C in the Cold section of Rotor B as a function of particle-projected area on a TEM negative. The dependence of composition on area is very weak. (b) Fe, Cr, and Mn content of M_3C in the Hot section of Rotor B as a function of particle-projected area on a TEM negative. Mn and Cr enrichment occurred in the Hot section carbides, and the larger particles appeared to contain less of these solute elements. However, the dependence of composition on area is still very weak.

pal change was in manganese content, with up to a 5 wt% increase, compared to the corresponding Cold section. The peak change in chromium content was around 3 wt%. Molybdenum, vanadium, and silicon changes were within the scatter band of the analyses.

The Hot section M_3C Fe/Cr ratio (Fig. 8) showed a roughly linear fall with the square root of exposure time, which might be expected of a diffusion-controlled reaction. The relationship derived was found to be:

$$M_3C\ Fe/Cr\ wt\% = -5.65 \times 10^{-3} \times t^{0.5}\,(h) + 5.03 \quad R = 0.92 \qquad \text{(Eq 1)}$$

where t = service exposure time in h and R = correlation coefficient.

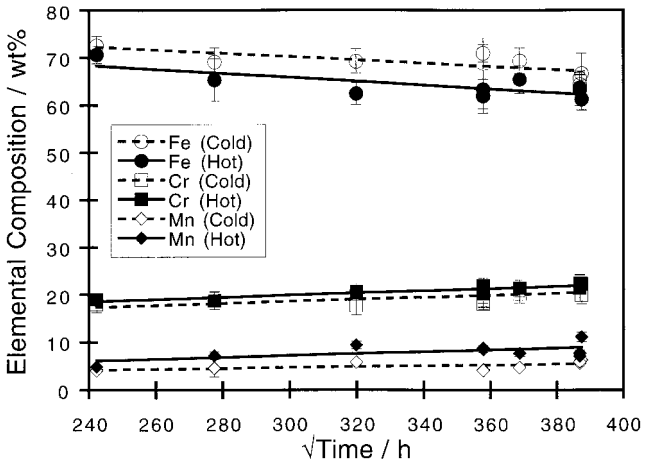

Fig. 7 Fe, Cr, and Mn content of M_3C carbides in the Hot and Cold sections of all the rotors studied. Compositional change (enrichment of Cr and Mn at the expense of Fe) occurs with time in both sections, being far more pronounced in the Hot section. Mo, V, and Si changes were minimal.

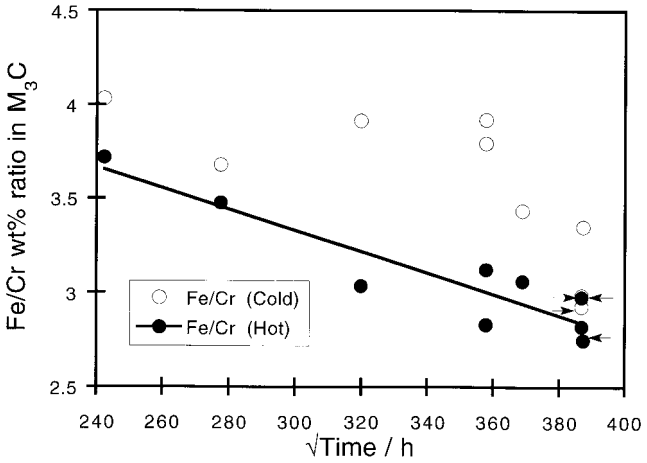

Fig. 8 M_3C Fe/Cr ratio of all the rotors as a function of $\sqrt{time}$. The Hot section ratio falls with a roughly linear dependence on $\sqrt{time}$, while the Cold section shows considerably more scatter and a much slower rate of change. Data points from Rotor F (arrowed) showed anomalous behavior (see text).

The corresponding plot for the Cold section Fe/Cr ratio showed considerable scatter, generally decreasing with time, but with no strong dependence on any particular time parameter. The Cold section data for Rotor F (Fig. 8—arrowed) were very similar to the corresponding Hot section data, unlike all the other rotors, which showed considerable differences between the corresponding sections.

The change in composition between the Hot and Cold section M_3C carbides (Hot-Cold) showed some interesting trends (Fig. 9). Silicon, vanadium, and molybdenum (not shown) were found to exhibit very little change, being within the scatter of the measurements. Up to ≈130 kh, both manganese and chromium increased in the M_3C at the expense of iron in a roughly linear manner when plotted against the square root of time. Linear regression on these data yielded the following expressions:

$$\Delta Cr\ wt\% \ -4.46 + 0.02 \times t^{0.5}\,(h) \quad R = 0.77 \text{ up to } \approx 130 \text{ kh} \qquad \text{(Eq 2)}$$

$$\Delta Fe\ wt\% \ 11.63 - 0.06 \times t^{0.5}\,(h) \quad R = 0.98 \text{ up to } \approx 130 \text{ kh} \qquad \text{(Eq 3)}$$

However, beyond ≈130 kh, the rate of chromium enrichment dropped abruptly, with a corresponding drop in the rate of iron depletion. Manganese, on the other hand, continued enriching up to 150 kh (the longest service exposure studied). Of the three data points which lay off this manganese trend, two were from Rotor F (Fig. 9—arrowed). This rotor showed somewhat unusual behavior, which is discussed in more detail in section "4. Discussion." The change in M_3C Mn composition was described by:

$$\Delta Mn\ wt\% = -5.28 + 0.03 \times t^{0.5}\,(h) \quad R = 0.98 \text{ up to } 150 \text{ kh} \qquad \text{(Eq 4)}$$

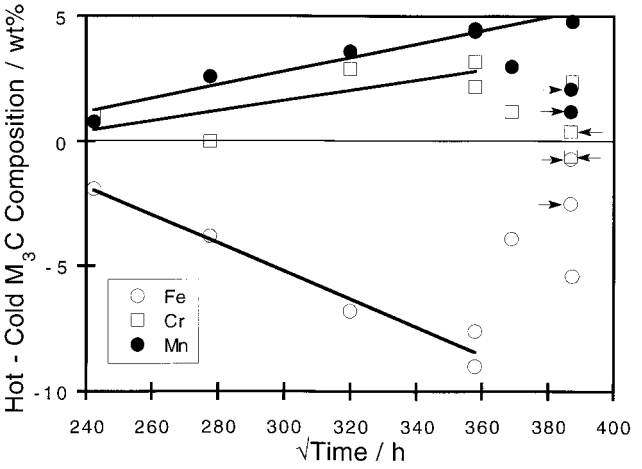

Fig. 9 Change in M_3C Fe, Cr, and Mn composition (Hot-Cold) as a function of $\sqrt{time}$. Mn showed the best trend, increasing linearly up to 150 kh. Fe and Cr changes tailed off after ≈100 kh. Data points for Rotor F (arrowed) showed anomalous behavior (see text).

Changes in the number of specific carbide types as a result of time at temperature were noted. These included secondary precipitation of MC and M_2C as a fine-scale precipitate (Fig. 3, 4), as well as increased numbers of H-type carbides and the development of chromium-rich carbides, such as $M_{23}C_6$. These higher alloy carbides were present in low numbers, even in very aged steels. It was not unusual to encounter (and ignore) 3 or 4 alloy-rich particles during analysis of 20 to 30 M_3C particles. Obtaining meaningful population statistics from such random particle analysis is very time-consuming, and has been shown to produce too much scatter to be of practical use (Ref 17).

An alternative approach tested here has been to carry out analysis of large areas of replicas containing many hundreds of individual carbide particles within a given field of view. While this technique does not permit the change in population of a specific carbide to be followed, it does allow general compositional changes brought about by alloy carbide precipitation and transformation to be followed. Maguire and Gooch (Ref 14) used a similar approach carrying out bulk analysis of electrolytically extracted carbides.

Changes in the average carbide composition were found in the Cold section replicas (Fig. 10a). The principal change was enrichment in the molybdenum content, and to a lesser degree the vanadium content, at the expense of iron. These changes were significant, with iron levels falling by over 10 wt% over 150 kh. This increasing level of molybdenum and vanadium is consistent with secondary precipitation of molybdenum-rich

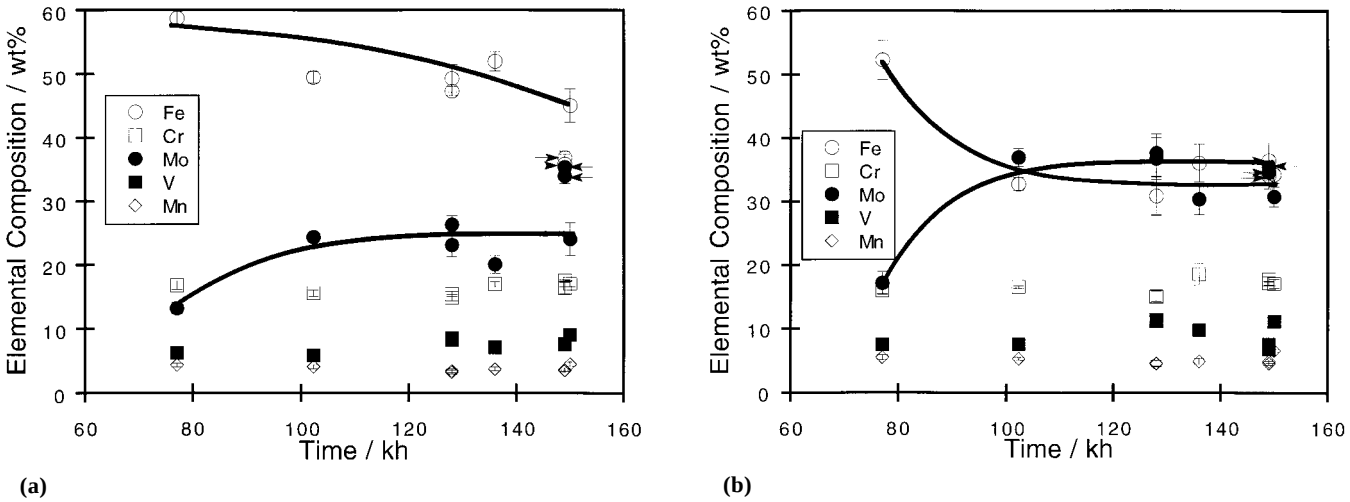

Fig. 10 (a) Average carbide compositions derived from large area analysis of replicas showing the change in the Cold section carbide composition as a function of service exposure. Mo enriches at the expense of Fe, with the values moving toward those of Rotor F (arrowed—see text). (b) Average carbide compositions derived from large area analysis of replicas showing the change in the Hot section carbide composition as a function of service exposure. Mo enrichment at the expense of Fe is largely complete at ≈100 kh, with the values converging to those of Rotor F (arrowed—see text).

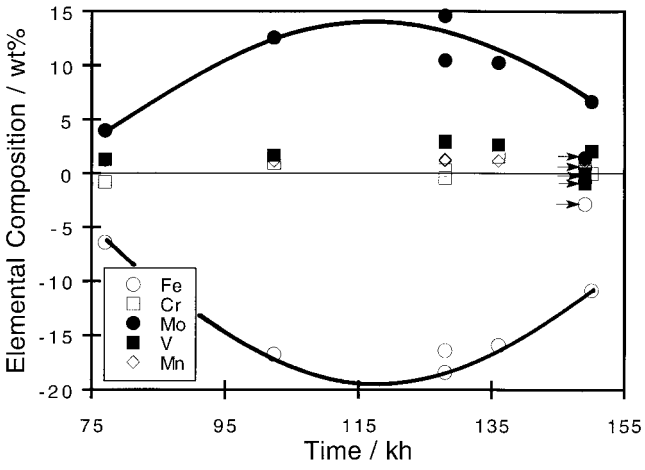

Fig. 11 Change in average carbide compositions (Hot-Cold) as a function of service exposure. Large increases in Mo levels at the expense of Fe occurred early on, although the rate of change decreased after ≈100 to 130 kh. Rotor F (arrowed) was extremely resistant to thermal modification.

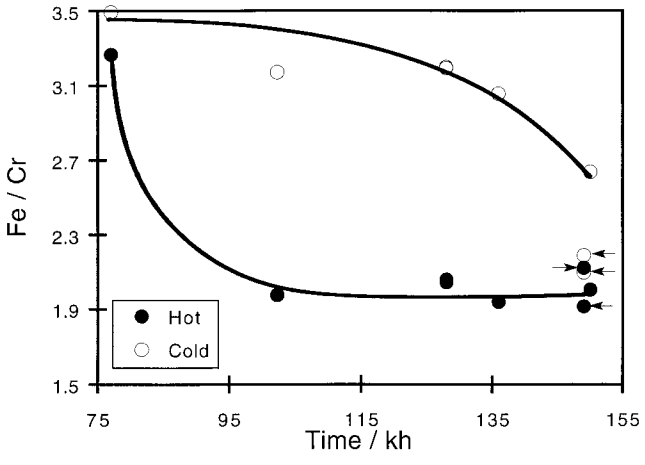

Fig. 12 Average carbide Fe/Cr ratio derived from large area analyses of the Hot and Cold sections of the rotors. Significant change occurs in the Cold section (≈350 °C), while in the Hot section (≈540 °C), the ratio stabilizes after ≈100 kh at the same value as that of Rotor F (see text).

M_2C and vanadium-rich MC. Chromium levels changed little in the Cold section, suggesting very limited enrichment of chromium in M_3C (confirmed earlier) in addition to limited precipitation of chromium-rich alloy carbides, such as $M_{23}C_6$. Clearly, an operating temperature of ≈350 °C is sufficient to bring about long-term compositional changes in 1CMV alloys. Rotor F showed unusual behavior. This rotor showed some of the best compositional uniformity, the least secondary precipitation, and average carbide compositions, derived from large area analysis, which were significantly richer in molybdenum and poorer in iron than any of the comparable exposure rotors (data points arrowed in Fig. 10a).

The average carbide compositions in the Hot sections of the rotors (Fig. 10b) showed much more marked depletion of iron and enrichment of molybdenum as a function of service exposure than the Cold sections, with changes of up to 20 wt%. However, the bulk of the change appeared complete by ≈100 kh, with both the average molybdenum and iron contents of the carbides leveling off at ≈35 wt%. The only other element that underwent any significant change was vanadium, increasing by 2 to 3 wt% over 150 kh exposure. Although up to ≈5 wt% Mn enrichment was observed in M_3C carbide (Fig. 9), this quite small change was swamped by the presence of the other carbide types. The average carbide compositions of all the longer-term exposure rotors converged to those of the Rotor F (Fig. 10b—arrowed).

The change in average carbide composition (Hot-Cold) as a function of service exposure (Fig. 11) showed that enrichment in molybdenum occurred at the expense of iron, with only minor enrichment in vanadium and little or no change in the other elements. The degree of change peaked at 100 to 130 kh, and then decreased. Rotor F was unusual in that it showed exceptional resistance to chemical change (data points arrowed in Fig. 11), with the largest compositional change between the Hot and Cold section of this rotor being ≈2 wt% Fe.

Plots of the Fe/Cr ratio derived from large area analysis (Fig. 12) showed the Cold section ratio was still falling at 150 kh, while in the Hot section, the change was largely complete by 100 kh, reaching a steady state Fe/Cr ratio of ≈2.0. This was very similar to the values measured in both the Hot and Cold sections of Rotor F (Fig. 12—arrowed).

4. Discussion

The general softening seen in the present results (Fig. 1) is similar to that observed for 1CMV alloys elsewhere (Ref 14, 18). The problem with such measurements is the high degree of scatter among various rotors. The present data set showed similar trends to the 1CMV softening curve derived by Gooch et al. (Ref 18), lying within the wide scatter bands inherent in such measurements. Hardness data were not available for Rotor F, so it was not possible to see if the anomalous microstructural and compositional behavior of this rotor was apparent in the hardness values. The scatter found in the typical hardness values of service-exposed rotors may correspond to 20% of the starting hardness, and may even involve some hardening (Ref 18). The largest difference seen here corresponded to only a 7% softening after 150 kh. Thermal softening measurements show quite limited sensitivity in relation to an effective time at temperature, and their use in remaining life assessment is therefore rather limited (Ref 18). However, as part of a broader condition assessment, where an attempt is made to place the rotor materials properties within the published scatter band of data, hardness measurements can be quite useful. The cause of the softening may be due to two microstructural changes: the coarsening and loss of coherency of the VC dispersion, and the loss of solid solution-strengthening molybdenum from the matrix (Ref 17). The present results showed extensive secondary fine-scale MC precipitation, which might be expected to harden rather than soften the material. However, considerable loss of molybdenum from solid solution was apparent, due to dramatic increases in the average carbide molybdenum content (Fig. 11), and this may contribute to the softening observed.

Norton and Strang (Ref 19) found the peripheral regions of 1CMV forgings to be predominantly upper bainite, where cooling rates from the austenitization temperature during quenching are highest. All the present rotors were examined at the rim, and showed a predominantly upper bainitic microstructure. Optical microscopy studies on the effect of aging on microstructure (Ref 3) have shown a similar result to that found here, namely that no differences between the Hot and Cold sections of even highly aged rotors can be detected using the technique, because it possesses insufficient resolution to detect the fine-scale changes. The principal carbides to develop were intragranular submicron carbides which were only apparent with the superior resolution of TEM.

All the carbide types identified in this study have been reported previously in 1CMV alloys (Ref 7). The TEM results showed that the predominant carbide type was iron-rich M_3C in the form of short laths (≈1 to 2 μm) or as rounded particles (≈1 μm) (Fig. 3a, 4a, 5) as has been noted elsewhere (Ref 4, 7, 9, 17). This carbide has been shown to comprise up to 95% of the typical grain boundary carbide population (Ref 14). Carbide types were identified on the basis of morphology and/or chemical composition (Ref 7, 17). Microstructures and carbide compositions were found to be similar both circumferentially and along the rotor axis at different isothermal locations on the rotors. This suggests that segregation effects were minimal within the rim regions of the rotors studied.

In the Hot sections, there was no marked spheroidization of lath carbides nor extensive precipitation along prior austenite grain boundaries. Occasional holes in replicas were present in replicas from both Hot and Cold sections, due to failed extraction of larger carbides. Joarder et al. (Ref 4) have reported large $M_{23}C_6$ precipitates forming along prior austenite grain boundaries in a rotor steel, after 200 kh at 521 °C. These carbides were not a major grain boundary feature in the present rotors, although such carbides were found intragranularly.

The secondary precipitation of carbides in a 1CMV alloy can be understood from the nature of the carbide product which forms during quenching from above the austenitization temperature. The carbide population found in upper bainite is predominantly iron-rich M_3C (Ref 4). This is the kinetically favored carbide, which has a non-equilibrium composition (Ref 11). However, subsequent tempering or in-service exposure results in diffusion of solute elements, principally chromium and manganese, into the carbide, and compositional changes occur, to yield a more thermodynamically stable prod-

uct (Ref 11, 17). Once a critical concentration of chromium is reached, decomposition of M_3C into $M_{23}C_6$ and/or M_7C_3 can occur (Ref 7). The carbide forming tendency of the various elements present in 1CMV has been shown to be V > Mo > Cr > Fe (Ref 8). This implies that molybdenum and vanadium would form the most thermodynamically stable carbides, and an equilibrium microstructure containing these elements will be rich in carbides. The nucleation of vanadium-rich MC on dislocations, and the subsequent nucleation of M_2C on MC particles to form H-type carbides, will occur during transition to an equilibrated microstructure.

The present analytical results showed that neither vanadium-rich MC nor molybdenum-rich M_2C compositions varied significantly as a function of time at temperature. Maguire and Gooch (Ref 14) have shown $M_{23}C_6$ to be compositionally stable. VC has also been reported to be resistant to aging effects in 0.5Cr-0.5Mo-0.25V alloys (Ref 20). Senior (Ref 17) has reported all carbides found in 1CMV to be compositionally stable, with the exception of M_3C. Carbide stability is temperature-dependent, as shown by Andrews et al. (Ref 8), and the equilibrium partitioning of elements into carbides such as M_3C also have a strong temperature dependence (Ref 10). One of the strengths of the present study is that it was performed on service-exposed material, and therefore does not raise the question of validity inherent in accelerated testing studies at elevated temperatures that are used to simulate long-term exposure. Such accelerated aging may lead to carbide populations which are quite different from those formed in service-exposed steels under conditions of lower temperature in conjunction with applied stress (Ref 8-10).

No attempt was made in this work to study the population dynamics of the fine-scale carbide phases, because such measurements on replicas are fraught with experimental error, owing to the uncertainty of carbide extraction, stemming from the variable etching responses of the various rotors and the inhomogeneous dispersion of MC and M_2C. The uniformity of the VC dispersion has been shown to be dependent on the M_3C precipitate distribution, with high M_3C concentrations suppressing MC formation (Ref 2, 19).

Because Evans et al. (Ref 21) had reported increased H-type carbide density in a 0.5Cr-0.5Mo-0.25V steel with time at temperature, an attempt to study the size and density of the H-type carbides was made in this investigation. However, the high degree of scatter associated with the measurements of both size parameters and densities (even those normalized to M_3C densities) was a major limitation, so no useful trends were obtained.

Analysis of M_3C composition showed it to be sensitive to time at temperature, with both manganese and chromium enriching at the expense of iron. Similar results for this carbide have been found in a wide range of low-alloy steels (Ref 12, 14, 15, 17). M_3C in 1CMV has been reported to exhibit a compositional range covering Fe/Cr ratios between 9 and 2.9, decreasing with time at temperature according to a cube root dependence (Ref 14).

One of the key aspects of this study, which differentiates it from many studies reported in the literature, is that it has studied a wide range of in-service rotors, each with a unique chemistry, thermo-mechanical history, and operating record. The experimental uncertainties in dealing with such a matrix of largely ill-defined parameters is not inconsiderable, in sharp contrast to carefully controlled accelerated laboratory studies carried out on single heats (e.g., Ref 14, 15). Uncertainty in operational data has been reported as a limiting factor in other studies of operational plant (Ref 21). Furthermore, this uncertainty precluded using time-temperature parameters because of the inherent sensitivity of such parameters to temperature. The nominal rotor design temperatures for the present data set (Table 1) are probably greater than the actual operating temperatures, because the majority of rotors spend only a very small percentage of their time at the design temperature, and many rotors are actually operated conservatively below design limits. This was apparent for Rotor F, where reasonably accurate operational data were available for the first 113 kh of operation. The putative LMP value based on design temperature yielded a value of 16,264 for this exposure, whereas the integrated LMP value from actual operational data was only 15,104. Furthermore, the rotor spent less than 10% of service at, or slightly above, the design temperature. The various trends established here that are based solely on exposure time tend to support the observation that the majority of the rotors in the present study operated at fairly similar temperatures, and that the differences in observed behavior are due mainly to differences in exposure time.

Analytical results for M_3C carbides from Cold sections of the rotor showed that some compositional change was occurring at ≈350 °C (Fig. 7, 8). A study by Joarder et al. (Ref 4) showed no changes occurring in a 23-year-old 1CMV rotor exposed at 288 °C. This suggests that the threshold for compositional change in 1CMV steel lies somewhere in the range 288 to 350 °C. It was hoped that the Cold sections of the rotor would be unaffected by temperatures of ≈350 °C, and would therefore afford a snapshot of the likely starting condition of the rotor. However, this clearly was not the case. Although it is possible to replicate regions of the rotor not exposed to steam, such as the coupling, these regions tend to be close to the bore. Data from Rotor D (not shown) indicated that the hardness, compositional, and microstructural differences between such a near-bore region and the rotor Cold section were greater than those between the Hot and Cold sections. Because of coring in the casting, and microstructural differences due to forging and heat treatment, the near-bore condition in a rotor is likely to be quite different from that of the near-rim condition (Ref 19).

The enrichment of chromium and manganese levels in M_3C during aging, as noted in the present work, has also been observed in a range of low-alloy steels (Ref 12, 15, 16). The extent of compositional modification was considerably lower in the Cold sections than in the Hot sections. Several workers (Ref 14, 16) have reported decreases in the Fe/Cr ratio of M_3C during aging, with a similar result obtained here (Fig. 8). These Fe/Cr ratio changes have often been reported to be a linear function of the cube root of time. However, there is no physical basis for such a relationship, because a diffusion-controlled reaction, which almost certainly drives the enrichment, would necessarily require a square root of time ($\sqrt{\text{time}}$) dependence (Ref 11).

The present Hot section M_3C Fe/Cr data were plotted as a function of $\sqrt{\text{time}}$ and showed a linear decline, from a value of 3.7 to 2.8. Maguire and Gooch (Ref 14) reported that M_3C may exhibit an Fe/Cr ratio as low as 2.9 before transformation to al-

loy carbides occurs. However, their aging work was carried out at 650 °C, and Mann et al. (Ref 12) have reported that higher M_3C enrichment levels occur at lower aging temperatures, albeit at a slower rate. It can be seen that the present data (≈540 °C) extend somewhat beyond the Fe/Cr = 2.9 threshold. Realistically, extrapolation of the Fe/Cr trend to longer service exposures may not be justified, owing to the instability of the carbide. Such relationships may therefore be of limited use in remaining life assessment.

Large area analysis showed some interesting trends, with evidence of significant modification of composition in the Hot sections and, to a lesser degree, in the Cold sections. The principal change was molybdenum enrichment at the expense of iron (Fig. 10), with slight vanadium enrichment also noted. Joarder et al. (Ref 4) have obtained similar results from aged rotor steels, following electrolytic extraction of the carbides. The extensive precipitation of molybdenum, and, to a lesser degree, vanadium, is not unexpected, as both these elements form very stable carbides (Ref 8), and the alloy contains 1 wt% Mo, but only 0.25 wt% V.

Assuming that the rotors contain ≈0.3 wt% C, which is a typical value for 1CMV rotors (Ref 3, 4, 19), and assuming that the bulk of this carbon is precipitated initially as M_3C (Ref 14, 17), then based on the present measurement of an M_3C chromium content of ≈20 wt% (Fig. 7), approximately 80% of the available chromium would be precipitated in the first instance as $(Fe_{\approx 0.8}, Cr_{\approx 0.2})_3C$, leaving only a limited amount in solid solution for enrichment and/or secondary precipitation. Because the M_3C carbide contains <5 wt% Mo, clearly far more molybdenum is left in solid solution to subsequently precipitate as M_2C, either in isolation or nucleated on MC particles to form H-type carbides.

Applying a similar argument to manganese, the typical alloy concentration for this element in 1CMV is 0.7 to 0.8 wt%. The manganese is principally associated with M_3C and does not form carbides in its own right. With a starting concentration of ≈5 wt% in the M_3C, only ≈20% of the available manganese is precipitated initially. In principle, this would suggest that there is sufficient manganese remaining in solid solution in the matrix to produce M_3C with a manganese content of up to ≈25 wt% (phase stability permitting). Mann et al. (Ref 12) have reported M_3C containing up to 9 wt% Mn in a 1Cr-0.5Mo steel, and a similar value has been reported by Afrouz et al. (Ref 22). In the present study, a peak M_3C manganese content of 11 wt% for Rotor G (150 kh) was observed (Fig. 7). It is clear that there is likely to be manganese available in solid solution in the matrix for considerably more manganese enrichment to occur in M_3C. It may be possible, therefore, to extrapolate the manganese enrichment trend observed here (Fig. 9). However, evaluation of longer service exposure material is required to evaluate whether the solubility limit of manganese in M_3C, or the instability of M_3C with respect to higher alloy carbides due to chromium enrichment, controls the carbide chemistry during extended aging.

The behavior of Rotor F was quite different from the other rotors studied in terms of the much lower degree of secondary precipitation of fine-scale carbide, the resistance to thermal modification, the composition of M_3C (Fig. 9), and the average carbide composition (Fig. 10-12). With regard to the Fe/Cr ratio, in the Cold section, the iron and molybdenum average carbide contents for Rotor F were ≈35 wt% (Fig. 10a), while the other rotors showed trends which were moving toward, but were still some way off, these levels. In the Hot section (Fig. 10b), compositional convergence of the average carbide compositions occurred at ≈100 kh, and changed very little thereafter. This compositional convergence was also apparent in the plot of average carbide Fe/Cr ratio (Fig. 12). The Hot section average carbide Fe/Cr ratio reached a steady state value of ≈2.0 after only 100 kh. Maguire and Gooch (Ref 14) have reported Fe/Cr ratios of 9 to 2.9 for M_3C, and 1.7 to 1 for M_7C_3. The present results are consistent with a mixed population of chromium-enriched M_3C along with chromium-rich alloy carbides ($M_{23}C_6$, possibly M_7C_3, along with other carbides such as M_2C which also contain varying levels of chromium). Such observations suggest that, unlike the other rotors, Rotor F had a near-equilibrated microstructure stemming from the manufacturing process, possibly due to extended tempering after forging. Unfortunately, the original manufacturing data for this rotor, as indeed for most of the rotors studied, was absent.

5. Conclusions

- Hardness measurements showed very limited softening (≈7%) after 150 kh service at ≈540 °C, with considerable scatter in the data. This limits the usefulness of hardness as a predictive tool in remaining life assessment. Microstructural and microanalytical investigation indicated significant carbide-induced loss of molybdenum from solid solution in the matrix, which would contribute to the observed softening.
- Microstructural characterization with optical microscopy yielded information on general microstructure and prior austenite grain size, but possessed insufficient resolution to detect the subtle microstructural changes that occurred in 1CMV rotor steels due to service exposure.
- TEM showed the principal microstructural effect of time at temperature to be secondary precipitation of fine-scale (<50 nm) MC and M_2C carbides. None of the rotors studied here showed extensive coarse carbide formation on prior austenite grain boundaries or associated carbide-denuded zones. From a microstructural point of view, all the rotors examined appeared likely to have good creep properties.
- Quantitative measurements of the changes occurring in the dimensions of H-type carbides due to time at temperature failed to identify any parameters which were dependent on service exposure.
- Compositional analysis showed that long-term exposure at temperatures of ≈350 °C in the steam exhaust sections of the rotors studied was sufficient to cause compositional change in carbides. Such regions cannot, therefore, be considered to be representative of the starting condition of the rotor.
- Compositional analysis of various carbide types showed that MC and M_2C carbide compositions were resistant to thermal modification. However, both the manganese and chromium contents of M_3C carbides were found to increase at the expense of iron with time at temperature in both Hot and Cold sections of the rotor. Manganese enrichment in

M_3C appeared to be the most useful, of all the compositional trends measured, for estimating effective time at temperature for remaining life assessment.

- Large area compositional analysis indicated changes in the average carbide compositions in both Cold (≈350 °C) and Hot (≈540 °C) sections of the rotors, with primarily molybdenum, and, to a much lesser degree, vanadium, increasing at the expense of iron. In the Cold sections, the changes in concentration were small and apparently incomplete after 150 kh. In the Hot sections, average compositional change appeared largely complete at ≈100 kh, with compositions equilibrating at levels very similar to those found in Rotor F.
- Rotor F, a rotor of Japanese origin, showed consistently different behavior in comparison to the other rotors studied. The major features of this rotor were: superior compositional uniformity of carbides throughout the rotor, resistance to secondary precipitation, and very good resistance to compositional change (both M_3C and average carbide composition). This behavior may be due to extended tempering of the rotor forging during manufacture, leading to a more equilibrated microstructure.

Acknowledgments

The authors are indebted to ESAA/ERDC for funding this project. Thanks go to AUSTA Electric, ECNZ, HRL Technology, Pacific Power, and Yallourn Power for providing access to rotors and operational information, and to M. Drew of Pacific Power for provision of some replicas and project support. The authors also wish to thank G.K. Smith, R. Finlay, and T. Nicholls of ANSTO for their technical assistance.

References

1. C.J. Moss, *Remaining Life Assessment of Turbine Rotors*, ESAA funded research (unpublished), 1996
2. G.J.P. Buchi, J.H.R. Page, and M.P. Sidey, Creep Properties and Precipitation Characteristics of 1%Cr-Mo-V Steels, *J. Iron Steel Inst.*, March 1965, p 291-299
3. N.S. Cheruvu and L.R. Malmfeldt, Metallurgical Characterization of a High-Pressure Rotor for Remaining Life Assessment after 26 Years of Service, *J. Eng. Gas Turbines Power*, Vol 112, 1990, p 543-549
4. A. Joarder, D.S. Sarma, and N.S. Cheruvu, Effect of Long-Term Service Exposure on Microstructure and Mechanical Properties of a CrMoV Steam Turbine Rotor Steel, *Metall. Trans. A*, Vol 22, 1991, p 1811-1820
5. V.P. Swaminathan, R. Viswanathan, and C.P. Clark, Material Property Studies of Two High-Pressure Turbine Rotors for Remaining Life Assessment, *J. Eng. Mater. Technol.*, Vol 116, 1994, p 19-26
6. A. Joarder, On the Bainite Structure in Cr-Mo-V Rotor Steel, *Steel Res.*, Vol 65, 1994, p 345-349
7. B.A. Senior, A Critical Review of Precipitation Behaviour in 1Cr-Mo-V Rotor Steels, *Mater. Sci. Eng. A*, Vol 103, 1988, p 263-271
8. K.W. Andrews, H. Hughes, and D.J. Dyson, Constitution Diagrams for Cr-Mo-V Steels, *J. Iron Steel Inst.*, May 1972, p 337-350
9. R.M. Goldhoff and H.J. Beattie, Jr., The Correlation of High Temperature Properties and Structures in 1Cr-Mo-V Forging Steels, *Trans. Metall. Soc. AIME*, Vol 233, 1965, p 1743-1756
10. X. Du, J.A. Whiteman, R.C. Thomson, and H.K.D.H. Bhadeshia, Modelling the Carbide Composition Changes in 1/2Cr1/2Mo1/4V Steel during Long-Term Tempering, *Mater. Sci. Eng. A*, Vol 155, 1992, p 197-205
11. H.K.D.H. Bhadeshia, Theoretical Analysis of Changes in Composition during Tempering of Bainite, *Mater. Sci. Technol.*, Vol 5, 1989, p 131-137
12. S.D. Mann, D.G. McCulloch, and B.C. Muddle, Characterization of Pearlitic Carbide in 1Cr-0.5Mo Steels, *Met. Mater. Trans. A*, Vol 26, 1995, p 299-307
13. J. Pilling and N. Ridley, Tempering of 2.25Pct Cr-1 Pct Mo Low Carbon Steels, *Metall. Trans. A*, Vol 13, 1982, p 557-563
14. J. Maguire and D.J. Gooch, Metallographic Techniques for Residual Life Assessment of 1CrMoV Rotor Forgings, *Proc. Int. Conf. Life Assessment and Extension*, The Hague, Netherlands, paper 2.5.4, June 13, 1988, p 116-124
15. R.C. Thomson and H.K.D.H. Bhadeshia, Changes in Chemical Composition of Carbides in 2.25Cr-1Mo Power Plant Steel: Part 1 Bainitic Microstructure, *Mater. Sci. Technol.*, Vol 10, 1994, p 193-203
16. A. Benvenuti, P. Bontempi, S. Corti, and N. Ricci, Assessment of the Thermal History in Elevated Temperature Components, *Mater. Char.*, Vol 36, 1996, p 271-278
17. B.A. Senior, "The Effects of Retempering on the Microstructure of Ferritic Steels Part 1: 1CrMoV Rotor Steel," CEGB Report No. TPRD/L/3220/R87, Feb 1988
18. D.J. Gooch, A. Strang, and S.M. Beech, Hardness Evaluation for Remanent Life Assessment of 1CrMoV Rotors, *Proc. Int. Conf. on Remaining Life Assessment*, Swansea, Wilshire and Evans, Ed., 1993, p 743-763
19. J.F. Norton and A. Strang, Improvement of Creep and Rupture Properties of Large 1%Cr-Mo-V Steam Turbine Rotor Forgings, *J. Iron Steel Inst.*, Feb 1969, p 193-203
20. R. Singh and S. Banerjee, Morphological and Compositional Changes of the Carbides in Cr-Mo-V Ferritic Steel, *Mater. Sci. Eng. A*, Vol 132, 1991, p 203-211
21. R.W. Evans, K.R. Williams, and B. Wilshire, A Microstructural Approach to Remanent Life Assessment, *Proc. 4th Int. Conf. on Remaining Life Assessment*, Swansea, Wilshire and Evans, Ed., 1990, p 1055-1064
22. A. Afrouz, M.J. Collins, and R. Pilkington, Microstructural Examination of 1Cr-0.5Mo Steel during Creep, *Met. Technol.*, Vol 10, 1983, p 461-463